Anomalous spin relaxation in graphene nanostructures on the high temperature annealed surface of hydrogenated diamond nanoparticles

V. L. Joseph Joly, [ID] †*[a] Kazuyuki Takai, [ID] ‡*[a] Manabu Kiguchi, [ID] [a] Naoki Komatsu [ID] [b] and Toshiaki Enoki [ID] *[a]

The electronic and magnetic structures of diamond nanoparticles with a hydrogenated surface are investigated as a function of annealing temperature under vacuum annealing up to 800–1000 °C. Near edge X-ray absorption fine structure (NEXAFS) spectra together with elemental analysis show successive creation of defect-induced nonbonding surface states at the expense of surface-hydrogen atoms as the annealing temperature is increased above 800 °C. Magnetization and ESR spectra confirm the increase in the concentration of localized spins assigned to the nonbonding surface states upon the increase of the annealing temperature. Around 800 °C, surface defects collectively created upon the annealing result in the formation of graphene nano-islands which possess magnetic nonbonding edge states of π-electron origin. Interestingly, extremely slow spin relaxation is observed in the magnetization of the edge state spins at low temperatures. The relaxation time is well explained in terms of a lognormal distribution of magnetic anisotropy energies instead of the classical Néel relaxation mechanism with a unique magnetic anisotropy energy, in addition to the contribution of the quantum mechanical tunnelling mechanism. The spin–orbit interaction enhanced by the electrostatic potential gradient created at the interface between the core diamond particle and surface graphene nano-islands is responsible for the slow spin relaxation.

Introduction

When diamond nanoparticles are annealed at high temperatures in inert Ar atmosphere or in vacuum, graphenization/graphitization along with the sp^3 to sp^2 conversion starts at their surfaces around 900 °C, then it proceeds into the interior of the particles at higher temperatures, and finally diamond nanoparticles are entirely graphitized around 1600 °C.[1–3] What interests us in the beginning of graphenization/graphitization is the formation of electrically conducting single layer graphene nanostructures on the surface of diamond nanoparticles with their interior being intact. Here, the electronic and magnetic structures of the graphene nanostructures formed on the surface vary in a wide range depending on their size and geometry. In particular, zigzag-shaped edges of the graphene nanostructures whose peripheries consist of a combination of zigzag and armchair edges possess spin-polarized nonbonding edge states of π-electron origin.[4–9] The edge-state spins interacting with each other through strong intra-zigzag edge ferromagnetic interactions together with intermediate strength inter-zigzag edge antiferromagnetic/ferromagnetic interactions take a wide range of magnetically ordered states depending on their mutual geometrical relationship.[10] In addition to the intrinsic magnetic structure in graphene nanostructures, in the case of nanostructures created on the diamond surface, interactions with the underlying diamond can work to modify the magnetic structures as well. In this context, we remind that the electronic holes created on the hydrogen-terminated diamond surface are subjected to the enhanced spin–orbit interaction owing to the formation of a large electrostatic potential gradient at the interface (Rashba effect),[11] even though the intrinsic spin–orbit interaction of carbon is extremely small (~ 5 cm^{-1}).[12] Actually, the hydrogen-terminated diamond surface induces charge transfer from the interior, giving rise to the accumulation of hole carriers in the vicinity of the surface.[13] As the result, the large electrostatic potential gradient created perpendicular to the surface works to enhance considerably the spin–orbit interaction at the surface. In general, carbon-based spins are easily subject to thermal fluctuations, due to the very weak magnetic anisotropy energy owing to a small intrinsic

[a] Department of Chemistry, Tokyo Institute of Technology, 2-12-1 Ookayama, Meguro-ku, Tokyo 152-8551, Japan. E-mail: josephjoly@stthomas.ac.in, takai@hosei.ac.jp, tenokih@gmail.com
[b] Graduate School of Human and Environmental Studies, Kyoto University, Sakyo-ku, Kyoto 606-8501, Japan
† Present address: Department of Chemistry, St. Thomas College, Thrissur, India.
‡ Present address: Department of Chemical Science and Technology, Hosei University, Tokyo, Japan.

spin–orbit interaction, resulting in less stable spin ordered states.[14] In contrast, we can stabilize the spin ordered state more and expect interesting collective phenomena in magnetic graphene nanostructures affected by the enhanced spin–orbit interaction on the hydrogenated diamond surface. Here, strongly correlated edge-state spins of graphene nanostructures under the effect of enhanced spin–orbit interactions are not only the important target to be challenged in carbon-based molecule magnetism but also offer new ingredients to cutting-edge spintronics applications.

With the motivation mentioned above, we have investigated the magnetic and electronic properties of surface-hydrogenated diamond nanoparticles and their annealing effect at high temperatures in relation to the formation of graphene nano-structures on the surfaces. We have observed the superpara-magnetic behavior of edge-state spins on the surface graphene nanostructures in the vicinity of annealing temperatures at which the nanostructures start developing. The anomalously slow magnetization relaxation observed together with non-Arrhenius-type temperature dependence is explained in terms of enhanced spin–orbit interactions for which the large electro-static potential gradient on the surface is responsible. The non-Arrhenius-type temperature dependence comes from a wide distribution of the magnetic anisotropy energies originating from the spin–orbit interaction.

Experimental

We employed diamond nanoparticles obtained after ball-milling of high-temperature, high-pressure synthesized dia-mond (Tomei Diamond Co. Ltd).[15] The sizes of the individual nanoparticles are distributed in a *ca.* 4–30 nm range according to SEM and STEM observations.[15] The average crystallite size of the diamond nanoparticles was estimated to be 11 nm from the peak width in powder X-ray diffraction using the Scherrer equation.[16] The diamond nanoparticles were covered by oxygen-containing surface functional groups such as OH and COOH, due to post-synthesis acid treatment.[15,17] The surface of the diamond nanoparticles was hydrogenated by heating at 600 °C in a hydrogen atmosphere, to replace the oxygen-containing functional groups with hydrogen. Hydrogenation of the surface was confirmed *via* FTIR spectra and elemental analysis. The diamond nanoparticles were heat-treated under high vacuum (10^{-6} Pa) in five different conditions (annealing temperature and time): 20 °C, 48 hours; 400 °C, 24 hours; 600 °C, 12 hours; 800 °C, 6 hours; 1000 °C, 4 hours, under which the samples obtained were named ND020, ND400, ND600, ND800, ND1000, respectively. The vacuum sealed NEX-AFS samples were opened to an ambient atmosphere for mounting on the sample holder. The NEXAFS sample chamber was baked under vacuum at about 200 °C for overnight, after mounting the samples. The carbon K-edge NEXAFS spectra of ND020, ND400, ND600, ND800 and ND1000 were measured using the total electron yield method, at the soft X-ray beam line BL-7A in the Photon Factory in the Institute of Materials

Structure Science, Tsukuba, Japan.[18] The intensity of NEXAFS spectra were normalized with respect to the edge jump at 340 eV, where the intensity was proportional to the amount of carbon. The photon energy was calibrated with respect to the C 1s to π* peak position of highly oriented pyrolytic graphite (HOPG) at 285.5 eV. Magnetization and magnetic susceptibility measurements were carried out in the temperature range from 2 to 300 K in the magnetic field up to 7 T using Quantum Design superconducting quantum interference device (SQUID). For SQUID measurements, ND020 and ND400 were wrapped in aluminium foil, ND600 in gold foil and ND800 in platinum foil. The wrapped samples were kept in a quartz tube and vacuum sealed after heat treatment. The typical sample weight was *ca.* 30 mg for the magnetization measurements. The background signal of the wrapping metal and quartz were subtracted to get the sample signal. The zero field cooled (ZFC) and field cooled (FC) measurements of magnetization gave identical results for all the samples and therefore all data given are in ZFC condi-tion. In order to investigate magnetization relaxation, time dependence of the magnetization was also measured. Since the samples showed slow magnetization relaxation at lower temperatures, the samples were allowed to thermally equili-brate at each temperature before the application of magnetic field in time dependence studies. Samples for X-band electron paramagnetic resonance (EPR) measurements were prepared in a "∩" shaped custom-made quartz tube with a vacuum sealing valve of Swagelok. One of the wings of the sample setup (heating-wing) was used for heating the sample and the other wing (measuring-wing) was the ESR sample tube. The sample was vacuum heat treated in the heating-wing, then vacuum sealed with the valve and carefully transported into the ESR wing. A single pristine sample heated at different temperatures was used for all the ESR studies. ESR measurements were carried out in heating runs in the range 4–300 K, using JEOL TE-200 X-band ESR spectrometer equipped with Oxford ESR910 helium continuous-flow cryostat. No ferromagnetic impurity signal was detected in ESR spectra for the diamond nanopar-ticle samples.

Results and discussion

The FTIR spectra of the hydrogenated diamond nanoparticle sample ND020 showed strong absorption at 2847 cm^{-1} of C–H symmetric stretching and 2928 cm^{-1} of C–H asymmetric stretching as depicted in Fig. 1, confirming surface hydrogena-tion of the diamond nanoparticles. From the elemental analysis result (C: 98.94%, H: 0.96%, O: 0.34%), the molar ratio is estimated to be C : H : O = 400 : 47 : 1, which suggests the successful surface hydrogenation in diamond nanoparticles in addition to the presence of a trace of remaining oxygen-containing functional groups on the surface. Let us estimate the surface coverage with hydrogen atoms in addition to the contribution of the oxygen-containing functional groups for the nanoparticle crystallite having a size of 11 nm, assuming that the diamond nanoparticles are spherical in shape with a
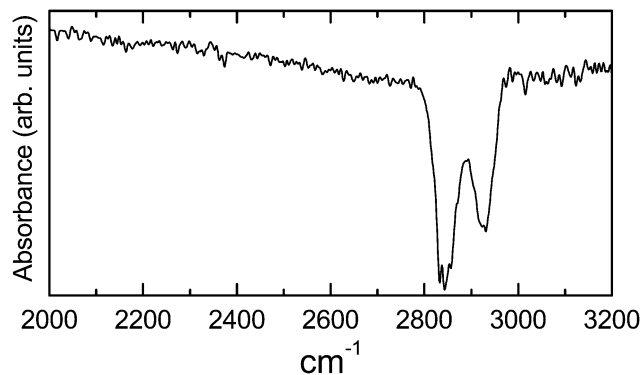
Fig. 1   FTIR spectrum of the pristine hydrogenated diamond nanoparticles (ND020). The absorptions at 2847 and 2928 cm^{-1} correspond to C–H symmetric and asymmetric stretching, respectively.

diameter of r = 11 nm (the observed crystallite size is 11 nm while the sizes of nanoparticles are distributed in 4–30 nm[15]). The total number of carbon atoms involved in an individual nanoparticle crystallite is given as $N_b = \left[\frac{4}{3}\pi(r/2)^3 \middle/ a^3 \right] 8$, where a = 0.3567 nm is the lattice constant of the fcc unit cell of diamond, in which 8 carbon atoms are involved. The number of surface carbon atoms is roughly given as $N_s = \left[4\pi(r/2)^2/a^2 \right] 2$, where we assume that the concentration of surface carbon atoms is represented by the (100) facet, in each of which 2 carbon atoms exist in the unit cell. Then the ratio is given as $N_s/N_b = \frac{3}{2}(a/r) = 4.86 \times 10^{-2}$ with $N_b = 1.23 \times 10^5$. From the result of the elemental analysis C : H : O = 400 : 47 : 1, the ratio of surface carbon atoms (N_{s-C}) is given as $400 \times 4.86 \times 10^{-2} = 16.3$, which is considerably smaller than the hydrogen content (47). Consequently, we can conclude that the surface is completely hydrogenated in good agreement with the FTIR spectrum shown in Fig. 1. The excess hydrogen concentration on the surface is suggestive of the presence of di- and tri-hydrogenated surface carbon sites in addition to the mono-hydrogenated sites. In addition, a part of the hydrogen atoms is considered to be involved as components of the remaining oxygen-containing surface functional groups.

Next, we track the change in the electronic structures upon high temperature annealing in a vacuum using the NEXAFS spectra. The normalized NEXAFS spectra of the diamond nanoparticle samples ND020, ND400, ND600, ND800, and ND1000 are given in Fig. 2. The bulk core-exciton peak in diamond is located at 289.3 eV[19–21] and the conduction band minimum for the surface carbon is ~0.60 eV below the bulk core-exciton peak as marked in Fig. 2. Three peaks P0, P1, and P2 are present in the gap in addition to the broad feature (around 288–289 eV) of σ*(C–C) just below the conduction band minimum as we can see in the expanded view of the lower energy region in the inset of Fig. 2. Fig. 3 shows the annealing temperature dependence of the intensity of the two peaks P0 and P1, which are obtained by deconvolution of the NEXAFS spectra. The ND020, ND400, and ND600 showed almost

identical features in the bulk band gap region of diamond (see Fig. 2).[20] This suggests that surface modification accompanying dehydrogenation does not take place up to 600 °C. The peak (P2) at 287.3 eV can be assigned to C(1s)–σ*(C–H$_x$) resonance (x = 1, 2, 3) in addition to the contributions of surface carbon atoms bonded to other functional groups such as –OH. ND800 and ND1000 showed a downward shift in this peak as more and more surface states are formed due to modification of the diamond surface.[20,22] It should be noted that the peak P2 still survives even in ND1000 as evidence that the surfaces remain still hydrogenated even at 1000 °C, though a part of the surfaces are dehydrogenated. A new peak (P1) appeared as a gap state at 285.2 eV corresponding to the C(1s)-π* transition of sp^2-bonded carbon, which showed a systematic increase in intensity with increased annealing temperature of above 800 °C. This is expected since the surface of diamond nanoparticles is slowly getting transformed into graphenic layers, at higher annealing temperatures. Another new gap state peak (P0) assigned to the nonbonding state[21] appeared at 282.7 eV from the surface core exciton above the annealing temperature of 800 °C, and its intensity increased upon the elevation of the annealing temperature. These findings together with the previous report[1,22–24] suggest that surface dehydrogenation takes place just above 800 °C, accompanied by surface graphenization. The graphenization induced by collective dehydrogenation allows the surface to form graphene nanostructures,[1–3] at the edge of which nonbonding edge states are created. As the result, the P0 peak appearing above 800 °C is assigned to the edge states in the graphene nanostructures on the surface. Here it should be noted that we cannot exclude the possibility of graphenization of the second layer beneath the uppermost layer in the present experimental result. However, it is rather difficult to graphenize the second layer since the annealing temperatures up to 1000 °C are well below the temperature of bulk graphitization (1600 °C). In other words, the contribution of the second layer is minor in comparison with that of the uppermost layer. In addition, the presence of graphene nanostructures on the second layer does not affect seriously the electronic structure of graphene on the surface due to the weakness of the interlayer interaction.[25]

The results of the ESR signal obtained for the pristine and high temperature annealed diamond nanoparticles are shown in Fig. 4 with the temperature dependence of the g-value and the peak-to-peak line width. The ESR signal obtained for the diamond nanoparticle samples did not show any of the characteristic features of either nitrogen related or Pauli paramagnetic spins of graphenic domains.[1,2,26–29] The narrow Lorentzian-type ESR line shape, along with the g-values close to the free spin (2.0023) and linewidths in the range of 1 mT, are characteristic features of the localized spins of carbon origin. The g-values were found to be almost temperature independent in the measurement temperature range as shown in Fig. 4. The linewidths were temperature independent and exhibited only a slight increase upon annealing up to 600 °C. Then it doubled above 600 °C. Finally, the linewidth reached 1.4–1.5 mT in ND800 and became weakly dependent on the
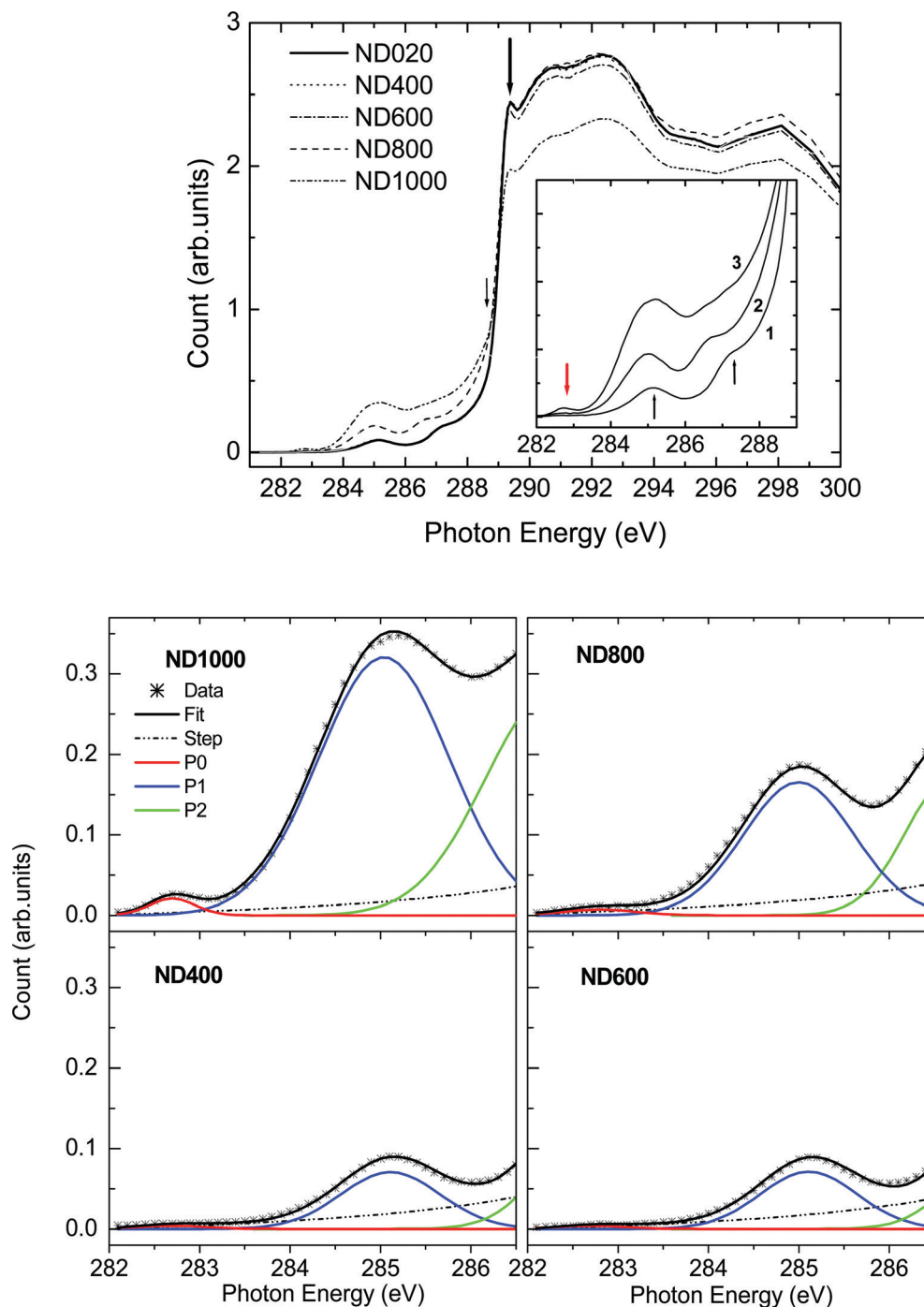
Fig. 2 (upper) The normalized NEXAFS spectra of diamond nanoparticle samples vacuum heat treated at 20 °C (ND020), 400 °C (ND400), 600 °C (ND600), 800 °C (ND800), 1000 °C (ND1000). The conduction band minimum for the surface carbon (thin short down arrow) and the bulk core exciton peak (thick long down arrow) are indicated. Inset: Expanded view of the bulk band gap region of ND020 (curve 1), ND800 (curve 2), and ND1000 (curve 3). The arrows roughly indicate the positions of P0 (red), P1 and P2 according to the photon energy. (lower) Deconvolution of the NEXAFS spectra below 286.5 eV with peaks P0 ($\sim$283 eV) and P1 ($\sim$285 eV). The experimental data and the fitting curves are given by the asterisk and thick solid line, respectively. The dotted line is the arctangent step function corresponding to the conduction band minimum (CBM), where the step function is centered at 289.67 eV with a width of 0.45 eV in all the cases, except for ND1000, where the step width is slightly higher (0.5 eV). The solid green line (P2) appearing above 285 eV is a part of the contribution from $\sigma^*(C-H_x)$ and other related peaks.

measurement temperature, in addition to the increase in the g-value. Taking into account that dehydrogenation starts on the surface above 800 °C, the discontinuous linewidth increase accompanied by the weak temperature dependence in the linewidth is suggestive of the important role of the edge-state spins created in an individual graphene nanostructure on the
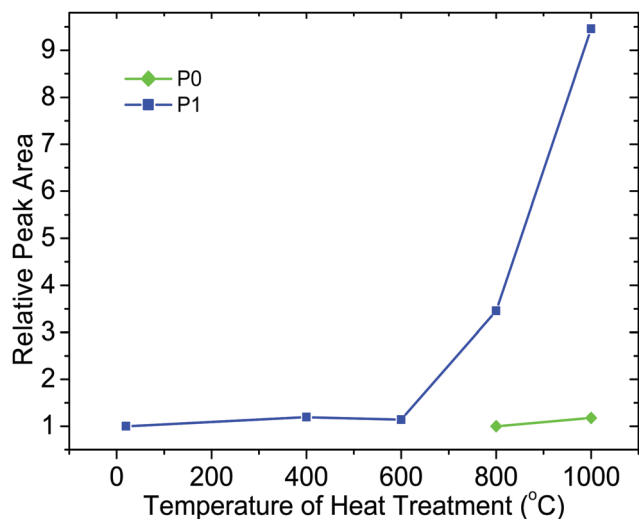
Fig. 3 The peak area of P0 and P1, relative to the peaks of the room temperature treated sample as a function of heat treatment temperature. It is clear that, up to 600 °C, there is no noticeable change in the peak area for the two peaks. Peak areas increased steadily and significantly on heating at 800 and 1000 °C.
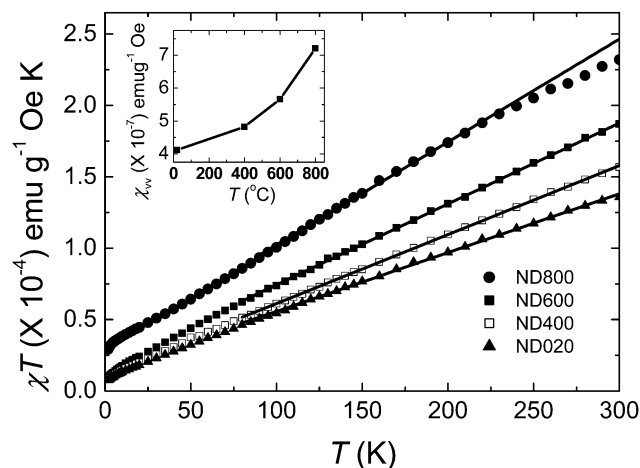

Fig. 5 Temperature dependence of the isothermal susceptibility of the diamond nanoparticle samples, measured at 1 T. The slopes are calculated from the straight line fits in the higher temperature region, as given in the graph. Inset: Heat-treatment dependence of the excess Van Vleck paramagnetic susceptibility.

surface and coupled with each other through strong magnetic interaction.[30] In this regard, we should remind the NEXAFS results, in which the nonbonding edge states (282.7 eV) of π-electron origin becomes evident above 800 °C. In addition, the fact that the linewidth increase is accompanied by the increase in the g-value tells us the signature of enhanced spin–orbit interaction in ND800, as will be discussed later.

The magnetic susceptibility showed paramagnetic behavior, consistent with the results of the ESR measurements. Here it should be noted that the bulk diamond has a net negative susceptibility -4.9×10^{-7} emu g^{-1} Oe^{-1} comprising the

core and the valence diamagnetism and the Van Vleck paramagnetism,[31,32] where the temperature independent Van Vleck paramagnetic susceptibility is estimated to be 5.5×10^{-7} emu g^{-1} Oe^{-1}.[31] Fig. 5 gives the temperature dependence of the isothermal susceptibility after subtracting the theoretical bulk susceptibility, -4.9×10^{-7} emu g^{-1} Oe^{-1}. The plot shows almost linear curves for all the samples with positive slopes, indicating the presence of an extra positive temperature independent susceptibility, which could either be due to Pauli or due to Van Vleck paramagnetism. Here, the possibility of temperature independent Pauli paramagnetism is excluded as the annealing temperatures are too low to form well defined graphene layers at the surface of diamond nanoparticles for the samples annealed below 600 °C or the Pauli paramagnetic
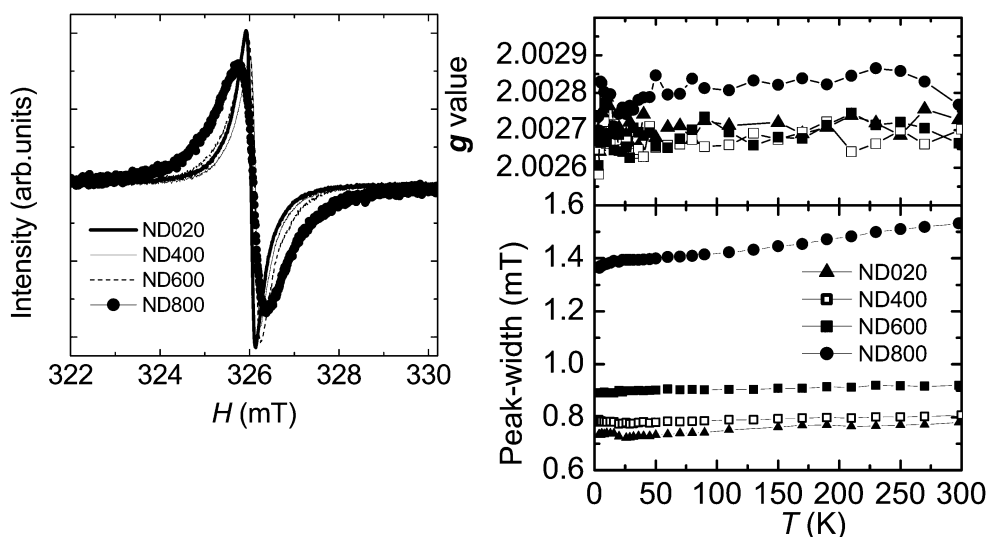

Fig. 4 ESR peak profiles (left) of the samples at room-temperature, measured using 0.01 mW power and 0.05 mT modulation. Temperature variation of the g values (right, top) and peak width (FWHM) after Lorentzian fit (right, bottom) of ND020, ND400, ND600, and ND800, measured at 0.01 mW microwave power.

susceptibility above 800 °C gives a negligible contribution in the graphene nanostructures, whose Fermi levels are located around the Dirac point.[7] In connection to the formation of graphene nano-structures, impurities having electron donating/accepting nature can work to enhance the Pauli paramagnetism. However, the estimated enhancement is two orders of magnitude smaller than the total susceptibility of the HTT800 sample at T = 100 K for example, even if the concentration of impurities, which might work as dopants, is in the range of 1%.[33] Therefore, this extra positive contribution is assigned to the enhancement in Van Vleck para-magnetic susceptibility, expressed as:[34]

$$\chi_{vv} = 2N \sum_{i,j} \frac{|\langle i|\mu_z|j\rangle|^2}{E_j - E_i} = \frac{B}{\beta E_g}, \quad (\beta \sim 1)$$

$$B = \sum_{i,j} \frac{|\langle i|\mu_z|j\rangle|^2}{E_j - E_i} \quad (1)$$

for $E_g \gg k_B T$, where N is the number of carbon atoms, $|i|\mu_z|j|$ is the nondiagonal matrix element of the magnetic moment operator connecting the occupied ground state i with the unoccupied excited state j, and E_g is the energy gap between the valence and conduction bands. In pure diamond, the occupied and unoccupied states correspond to the valence and conduction bands, respectively. Accordingly, the Van Vleck paramagnetism contribution is negligi-bly small in pure diamond as the energy gap is large (E_g = 5.47 eV). When impurity and/or surface states are created in the energy gap region in defective diamond or surface-modified diamond, the excitations from the occupied ground state to the unoccupied excited state, both of which distribute as impurity and/or surface states in the energy gap between the valence and conduction bands, contribute to the enhancement in the Van Vleck paramag-netism.[31,32,34] As the consequence, the enhancement in the Van Vleck term observed in the present experiment originates from the growing number of surface states located in the energy gap of the diamond nanoparticles. The high temperature annealing induces the rearrangement of the surface even before dehydrogenation starts, resulting in the increase in the surface states and dehydro-genation taking place above 800 °C participates in the creation of surface states, in which the edge-states of graphene nanostructures are involved. The modification of the NEXAFS spectra in the σ* region along with the low energy shift of peak P2 is related to the structural modification accompanied by surface states. Here, it should be noted again that graphene nanostructures created on the surface particularly for the sample heat-treated above 800 °C gives an additional contribution of orbital diamagnetic susceptibility of π-electron origin to the susceptibility observed. In the previous work,[2] the orbital contribution is estimated as ∼10^{-6} emu g^{-1}. Taking into account the fraction of surface carbon atoms, N_s/N_b = 4.86 × 10^{-2}, a part of which is graphenized, the contribution of the orbital diamagnetism ($\leq 5 \times 10^{-8}$ emu g^{-1}) is negligible enough to make a correction necessary for the Van Vleck paramagnetism.

The creation of surface states together with dehydrogenation at the surface gives temperature dependent Curie type suscepti-bility as well from s =1/2 paramagnetic spins, as observed in the low temperature range, where the Van Vleck magnetization is

1–2 orders of magnitude smaller. Fig. 6 shows the magnetiza-tion data at 2 K of ND020, ND400, ND600, and ND800 and the s = 1/2 Brillouin function fits. The Curie type paramagnetic spin concentration obtained from s =1/2 Brillouin function fit at 2 K are 1.1 × 10^{19} g^{-1}, 1.2 × 10^{19} g^{-1}, and 1.5 × 10^{19} g^{-1} for ND020, ND400 and ND600, respectively. Taking into account that the g-value is independent of the annealing temperature in this annealing temperature range up to 600 °C, the spin species are in the same origin in this annealing temperature range. The slight increase in the spin concentration together with a slight broadening of the ESR linewidth is suggestive of a slight rearrangement and increase in the number of the magnetic surface states which are present in the pristine hydrogenated diamond nanoparticles. It should be noted that the surface carbon atoms to which hydrogen atoms are bonded are not regularly arranged so that many defects are present as a source of surface states. After annealing at 800 °C, close to the dehydrogenation temperature, the Curie-type spin concen-tration of diamond nanoparticles (ND800) showed a threefold increase (see the inset of Fig. 6), reinforcing the fact that the Curie type surface spins originate from the nonbonding edge states in the peripheries of graphene nanostructures on the surfaces.[4–10]

In carbon-based magnetic materials, in which the magnetic carbon atom has an extremely weak magnetic anisotropy owing to its weak spin–orbit interaction (5 cm^{-1}),[12] magnetic responses are so rapid that the time dependent relaxation is not observed in general in static magnetic susceptibility and magnetization.[1] However, slow magnetization relaxation was observed at low temperatures in the high temperature annealed diamond nanoparticles in the present experiments. Fig. 7 shows the time dependence of the magnetization on increasing the magnetic field from 1 to 4 T at 2 K, where the magnetization at 1 T was allowed to saturate before the increase to 4 T. The
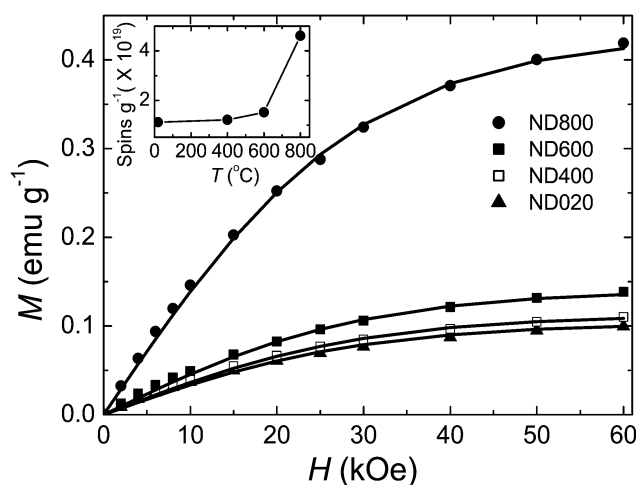
Fig. 6 Brillouin function fit (solid line) to the magnetization data at 2 K of ND020, ND400, ND600, and ND800 with s = 1/2. The diamagnetic contribution of bulk diamond is subtracted before fitting. Inset: The number of spins obtained after Brillouin function fit as a function of vacuum heat-treatment temperature.
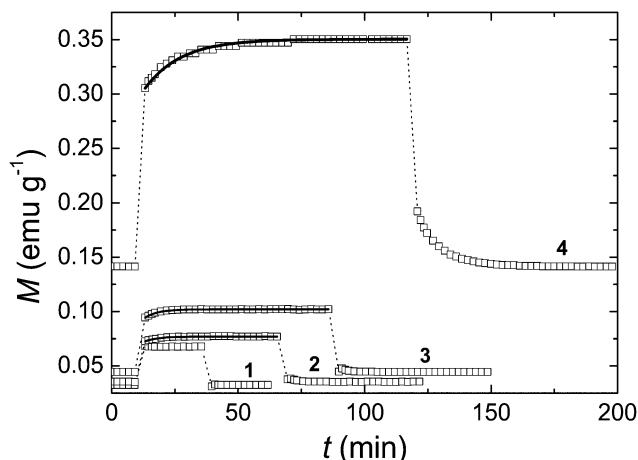
Fig. 7 Time dependence of magnetization at 2 K for the samples ND020 (curve 1), ND400 (curve 2), ND600 (curve 3), and ND800 (curve 4) kept in thermal equilibrium at 1 T, followed by an increase in field to 4 T (indicated by the sudden jump in the magnetization). After attaining the saturation in the magnetization, the field is reduced to 1 T (indicated by the sudden drop in magnetization). The dotted lines are guide to the eyes and the thick lines are the exponential fit. The rise/fall time of the magnetic field is 3 min between 1 and 4 T.

room-temperature evacuated pristine sample (ND020) showed no detectable time dependence of the static magnetization down to 2 K. In contrast, ND400 and ND600 exhibited detectable time dependence, which increased dramatically in ND800. The magnetization dynamics can be fitted with an exponential function given by

$$M_z(t) = M_0 \left[1 - e^{-\frac{t}{\tau}} \right], \quad (2)$$

where M_0 is the equilibrium magnetization and τ is the relaxation time constant. From the fit, ND400 and ND600 gave the same τ as 300 ± 20 s, and ND800 gave an extremely long 850 ± 20 s. Since the number of Curie-type paramagnetic spins increased upon high temperature annealing and it became three times larger than that in the pristine sample for ND800, the observed long time relaxation can be attributed to the surface spins formed by high temperature annealing and subsequently by the dehydrogenation above 800 °C. Here it should be reminded that the diamond nanoparticles, whose surfaces are not hydrogenated, have no detectable time dependence in the magnetization even if graphene nanostructures are created at 900 °C, at which only the surfaces are graphitized with the interior of the diamond nanoparticles being intact.[2] In other words, it is the important requisite to observe the long time dependence that graphene nanostructures and hydrogenated surface regions coexist on the diamond nanoparticles. A hydrogenated surface works to accumulate conducting hole carriers at the interface between the surface and the interior in diamond,[13] resulting in the enhancement of the spin–orbit interaction which in turn is due to the sharp electrostatic potential gradient created perpendicular to the surface (Rashba effect).[11] The deviation of the g-value from the free electron

spin observed in the ESR signal for ND800 is an important signature for the enhancement of the spin–orbit interaction. Taking into account the enhanced spin–orbit interaction in the spins on the surface, the enhancement of the magnetic anisotropy is responsible for the extremely long relaxation time observed in the magnetization. In particular, the edge-state spins in the graphene nanostructures on the surface annealed at 800 °C can have more elongated relaxation time as the edge-state spins are interacting with each other through strong intra-zigzag edge ferromagnetic interactions.[30] In other words, collectively interacting spins created around the graphene edge regions are subjected to the slow dynamics, for which an interplay between the exchange interaction and strong magnetic anisotropy is responsible. This can be explained in terms of superparamagnetic behavior.[35,36]

In order to understand the mechanism behind the slow magnetization relaxation further in details, the temperature dependence of τ at low temperatures was studied for ND800, in which graphene nanostructures are formed on the surface with the localized spins being assigned to the edge-state spins. In the measurement temperature range (2–6 K), the sample was kept in thermal equilibrium at 0.2 T at each temperature, followed by an increase in field to 4 T (see Fig. 8). The value of $1/\tau$ obtained after fitting the above relaxation equation to the data of Fig. 8 is plotted against temperature in Fig. 9(a). $1/\tau$ was found to be linearly dependent on the temperature, and it deviated upward from the linear dependence at the lowest temperature (2 K). The observed linear temperature dependent $1/T_1$ is not agreeable with that expected in superparamagnets with Arrhenius-type Néel relaxation[37] given as

$$\frac{1}{\tau} = \frac{1}{\tau_0} \exp\left(-\frac{E_a}{k_B T} \right), \quad (3)$$

where the activation energy $E_a = KS$ is the product of the magnetic anisotropy density K and the surface area S of graphene nanostructures. Here we should remember that the
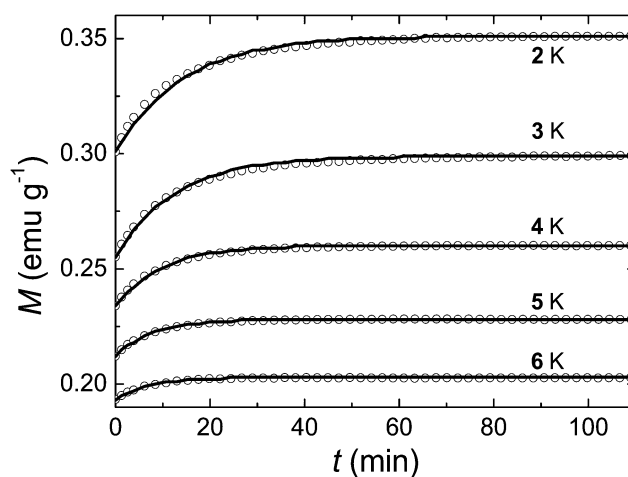

Fig. 8 Temperature dependence of relaxation phenomenon in the range of 2–6 K for ND800 kept in thermal equilibrium at 0.2 T followed by an increase in field to 4 T. The thick lines are the exponential fit to the data.

graphene nanostructures distributed on the surfaces of the diamond nanoparticles are not regularly arranged. The surface carbon atoms of the pristine unannealed diamond nanoparticles are terminated in a disordered manner by hydrogen atoms with mono-, di- and tri-hydrogenated sites and also by other functional groups such as oxygen-containing functional groups. Therefore, the high temperature annealing above 800 °C is affected by this structural randomness of the surfaces, resulting in a wide distribution of the sizes and shapes of graphene nanostructures grown on the surface. In addition, the interactions between the surface graphene nanostructures and the underneath diamond nanoparticles, which remain partly hydrogenated, vary randomly. Accordingly, the edge state spins distributed around the edge region of the graphene nanostructures have a large variation in their environments. This means that both the strength of the magnetic anisotropy and collective features of the edge-state spins are widely distributed, resulting in the wide distribution of the superparamagnetic activation energy E_a in the magnetization relaxation. In an assembly of superparamagnets, in which the activation energies are widely distributed, it is known that the distribution obeys the lognormal distribution.[36,37] In addition, the experimental results shown in Fig. 8 indicates the relaxation rate $1/\tau$ to be extrapolated to a finite value at $T = 0$ K, suggesting the presence of a non-thermal (tunnelling) contribution $1/\tau_{tunnel}$ in the relaxation rate. As a consequence, the observed relaxation time averaged over the whole sample is described by the following equation:

$$\left\langle \frac{1}{\tau(E_a)} \right\rangle = \frac{1}{\tau_0} \int_0^\infty \exp\left(-\frac{E_a}{k_B T}\right) P(E_a) dE_a + \frac{1}{\tau_{tunnel}}, \qquad (4)$$

where $P(E_a)$ is the lognormal distribution function:

$$P(E_a) = \frac{1}{\sqrt{2\pi}\sigma E_a} \exp\left[\frac{-\left\{\ln\left(\frac{E_a}{\mu}\right)\right\}^2}{2\sigma^2}\right], \qquad (5)$$

with μ and σ connected to the average and the standard deviation of E_a by $\langle E_a \rangle = e^{\left(\mu + \frac{\sigma^2}{2}\right)}$ and $\sqrt{\langle (\Delta E_a)^2 \rangle} = \sqrt{(e^{\sigma^2} - 1)e^{2\mu+\sigma^2}}$, respectively. The magnetization relaxation time is well explained with the thermal contribution described by the lognormal distribution in the activation energies E_a together with the tunnelling contribution as shown in Fig. 9. The average and the deviation of the activation energy are given as $\langle E_a \rangle = 13.3$ K, $\sqrt{\langle (\Delta E_a)^2 \rangle} = 4.5$ K, respectively. The tunnelling ratio is estimated as $1/\tau_{tunnel} = 1.1 \times 10^{-3}$ s^{-1}. The large standard deviation of the activation energy compared with the average comes from a wide range of structural randomness in the magnetic graphene nanostructures created on the surfaces of the diamond nanoparticles. Here, not only the wide distributions of the sizes and shapes of the nanostructures but also the wide distribution of the electrostatic potential gradients created by the hole carriers at the surfaces are responsible for the activation energy distribution. It should be noted that the large contribution of the tunnelling process to the
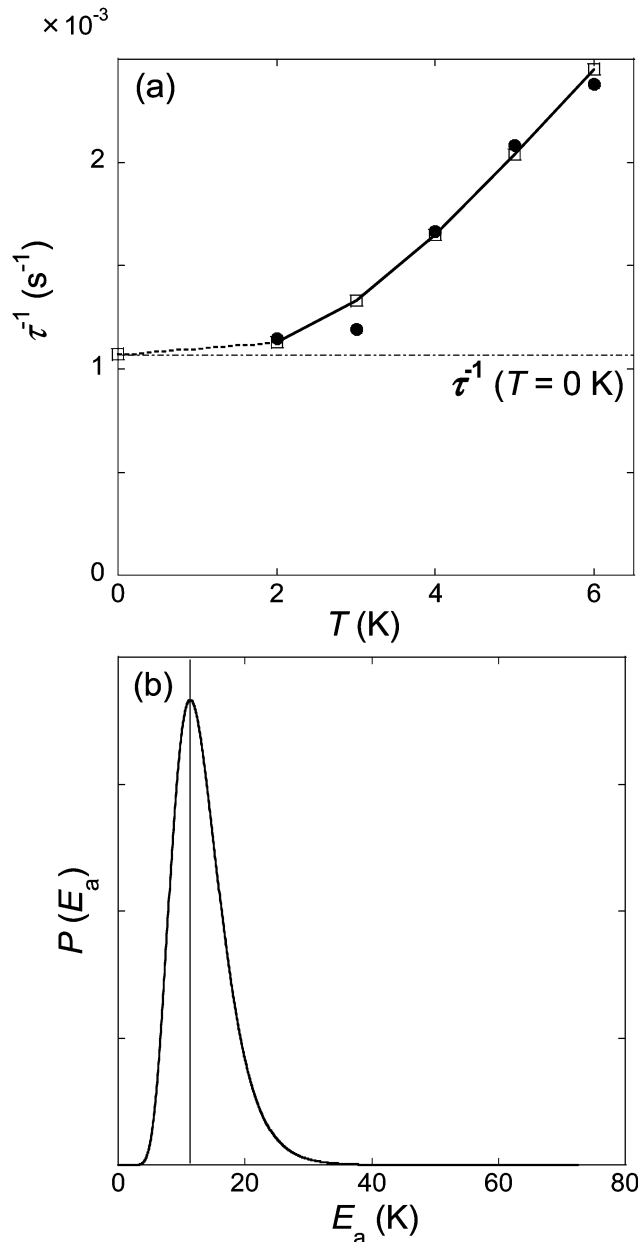

Fig. 9 (a) Temperature dependence of the magnetization relaxation time τ in the range of 2–6 K for ND800 kept in thermal equilibrium at 0.2 T followed by an increase in field to 4 T. Full circles and open squares connected by the solid line are the experimental data and the values obtained by fitting with the lognormal distribution of the activation energy E_a, respectively. The tunnelling term is estimated as $1/\tau(T = 0$ K$) = 1.1 \times 10^{-3}$ s. (b) The lognormal distribution function $P(E_a)$ of the activation energy. The average and the deviation are given as $\langle E_a \rangle = 13.3$ K and $\sqrt{\langle (\Delta E_a)^2 \rangle} = 4.5$ K, respectively.

magnetization relaxation is suggestive of the quantum mechanical feature of the spins in the graphene nanostructures.

Conclusions

The annealing temperature dependence of the electronic and magnetic structure in diamond nanoparticles with their surface

hydrogenated have been investigated as a function of annealing temperature under vacuum annealing up to 800 °C. The near-edge X-ray absorption fine structure (NEXAFS) spectra together with elemental analysis show the successive creation of defect-induced nonbonding surface states at the expense of hydrogen atoms terminating the surface carbon atoms as the annealing temperature is increased. Magnetizations and ESR spectra confirm the increase in the concentration of localized spins assigned to the surface states upon the increase of the annealing temperature. Around 800 °C, defects collectively created upon annealing result in the formation of graphene nano-islands, around the peripheries of which magnetic nonbonding edge states of π-electron origin are formed. Interestingly, extremely slow spin relaxation is observed in the magnetization of the edge state spins at low temperatures. The relaxation time cannot be explained simply in terms of the classical Néel relaxation mechanism with a unique magnetic anisotropy energy but is well explained in terms of a combination of the thermal activation process with a wide distribution of the magnetic anisotropy energies and the tunnelling process. The former can be fit with the lognormal distribution of magnetic anisotropy energies due to the disordered nature of graphene nanostructures on the surfaces of diamond nano-particles, while the latter comes from the quantum mechanical nature of the spins in graphene nanostructures. In the former, the spin–orbit interaction enhanced by the electrostatic potential gradient created at the interface between the hydrogenated diamond particles and surface graphene nanostructure plays a key role in the extremely slow relaxation. The slow relaxation makes the tunnelling process stand out more clearly at low temperatures.

Conflicts of interest

There are no conflicts to declare.

Acknowledgements

References

1 O. E. Andersson, B. L. V. Prasad, H. Sato, T. Enoki, Y. Hishiyama and Y. Kaburagi, *et al.*, *Phys. Rev. B: Condens. Matter Mater. Phys.*, 1998, **58**(24), 16387–16395.

2 B. L. V. Prasad, H. Sato, T. Enoki, Y. Hishiyama, Y. Kaburagi and A. M. Rao, *et al.*, *Phys. Rev. B: Condens. Matter Mater. Phys.*, 2000, **62**(16), 11209–11218.

3 N. Tokuda, M. Fukui, T. Makino, D. Takeuchi, S. Yamsaki and T. Inokuma, *Jpn. J. Appl. Phys.*, 2013, **52**(11R), 110121.

4 M. Fujita, K. Wakabayashi, K. Nakada and K. Kusakabe, *J. Phys. Soc. Jpn.*, 1996, **65**(7), 1920–1923.

5 Y. Kobayashi, K. Fukui, T. Enoki, K. Kusakabe and Y. Kaburagi, *Phys. Rev. B: Condens. Matter Mater. Phys.*, 2005, **71**(19), 193406.

6 P. Ruffieux, S. Wang, B. Yang, C. Sánchez-Sánchez, J. Liu and T. Dienel, *et al.*, *Nature*, 2016, **531**(7595), 489–492.

7 T. Enoki and T. Ando, *Physics and Chemistry of Graphene*, Jenny Stanford Publishing, 2nd edn, 2019.

8 R. Masrour and A. Jabar, *Superlattices Microstruct.*, 2016, **98**, 78–85.

9 R. Masrour and A. Jabar, *Synth. Met.*, 2021, **273**, 116694.

10 T. Enoki and K. Takai, *Solid State Commun.*, 2009, **149**(27), 1144–1150.

11 G. Akhgar, O. Klochan, L. H. Willems, van Beveren, M. T. Edmonds and F. Maier, *et al., Nano Lett.*, 2016, **16**(6), 3768–3773.

12 K. Matsubara, T. Tsuzuku and K. Sugihara, *Phys. Rev. B: Condens. Matter Mater. Phys.*, 1991, **44**(21), 11845–11851.

13 F. Maier, M. Riedel, B. Mantel, J. Ristein and L. Ley, *Phys. Rev. Lett.*, 2000, **85**(16), 3472–3475.

14 Y. Shibayama, H. Sato, T. Enoki and M. Endo, *Phys. Rev. Lett.*, 2000, **84**(8), 1744–1747.

15 Y. Morita, T. Takimoto, H. Yamanaka, K. Kumekawa, S. Morino and S. Aonuma, *et al.*, *Small*, 2008, **4**(12), 2154–22157.

16 H. P. Klug and L. E. Alexander, *X-ray Diffraction Procedures*, John Wiley and Sons, New York, 1954.

17 A. Krueger, *Chem. – Eur. J.*, 2008, **14**(5), 1382–1390.

18 K. Amemiya, H. Kondoh, T. Yokoyama and T. Ohta, *J. Electron Spectrosc. Relat. Phenom.*, 2002, **124**(2), 151–164.

19 J. F. Morar, F. J. Himpsel, G. Hollinger, G. Hughes and J. L. Jordan, *Phys. Rev. Lett.*, 1985, **54**(17), 1960–1963.

20 J. F. Morar, F. J. Himpsel, G. Hollinger, J. L. Jordon, G. Hughes and F. R. McFeely, *Phys. Rev. B: Condens. Matter Mater. Phys.*, 1986, **33**(2), 1346–1349.

21 K. Bobrov, G. Comtet, G. Dujardin, L. Hellner, P. Bergonzo and C. Mer, *Phys. Rev. B: Condens. Matter Mater. Phys.*, 2001, **63**(16), 165421.

22 J. B. Cui, J. Ristein and L. Ley, *Phys. Rev. B: Condens. Matter Mater. Phys.*, 1999, **59**(8), 5847–5856.

23 G. Kern, J. Hafner and G. Kresse, *Surf. Sci.*, 1996, **366**(3), 464–482.

24 A. V. Hamza, G. D. Kubiak and R. H. Stulen, *Surf. Sci.*, 1990, **237**(1), 35–52.

25 K. Sakai, K. Takai, K. Fukui, T. Nakanishi and T. Enoki, *Phys. Rev. B: Condens. Matter Mater. Phys.*, 2010, **81**(23), 235417.

26 E. C. Reynhardt, G. L. High and J. A. van Wyk, *J. Chem. Phys.*, 1998, **109**, 8471–8477.

27 J. A. van Wyk, E. C. Reynhardt, G. L. High and I. Kiflawi, *J. Phys. D: Appl. Phys.*, 1997, **30**(12), 1790–1793.

28 A. I. Shames, A. M. Panich, W. Kempiński, A. E. Alexenskii, M. V. Baidakov and A. T. Dideikin, *et al.*, *J. Phys. Chem. Solids*, 2002, **63**(11), 1993–2001.

29 K. Iakoubovskii, M. V. Baidakova, B. H. Wouters, A. Stesmans, G. J. Adriaenssens and A. Y. Vul', *et al.*, *Diamond Relat. Mater.*, 2000, **9**(3), 861–865.

30 K. Wakabayashi, M. Sigrist and M. Fujita, *J. Phys. Soc. Jpn.*, 1998, **67**(6), 2089–2093.

31 S. Hudgens, M. Kastner and H. Fritzsche, *Phys. Rev. Lett.*, 1974, **33**(26), 1552–1555.

32 J. Heremans, C. H. Olk and D. T. Morelli, *Phys. Rev. B: Condens. Matter Mater. Phys.*, 1994, **49**(21), 15122–15125.

33 S. Ikehata, T. Moritomo, H. Suematsu and S. Tanuma, *Synth. Met.*, 1985, **12**(1), 313–317.

34 A. V. Nikolaev and B. Verberck, *Carbon-based Magnetism*, Elsevier, Amsterdam, 2006, p. 245.

35 J. L. Dormann and D. Fiorani, *Magnetic Properties of Fine Particles*, Amsterdam: North Holland, 1st edn, 1992.

36 B. Barbara, L. C. Sampaio, A. Marchand, O. Kubo and H. Takeuchi, *J. Magn. Magn. Mater.*, 1994, **136**(1), 183–188.

37 Y. Komorida, M. Mito, H. Deguchi, S. Takagi, T. Tajiri and A. Millán, *et al.*, *J. Magn. Magn. Mater.*, 2010, **322**(15), 2117–2126.